ELSEVIER

Contents lists available at ScienceDirect

Hearing Research

journal homepage: www.elsevier.com/locate/heares



A simple electrical circuit model for impedance spectroscopy with cochlear implant electrodes



Merle Sehlmeyer a,*,#, Mit B. Bhavsar b,#, Stefan Zimmermann a, Hannes Maier b

- ^a Leibniz University Hannover, Institute of Electrical Engineering and Measurement Technology, Department of Sensors and Measurement Technology, Appelstr. 9A, Hannover 30167, Germany
- b Hannover Medical School, Department of Otolaryngology/NIFE and Cluster of Excellence "Hearing4all", Stadtfelddamm 34, Hannover 30625, Germany

ARTICLE INFO

Keywords:
Cochlear implant
Impedance spectroscopy
Electrical equivalent circuit
Electrode-electrolyte interface

ABSTRACT

Although cochlear implants are an established method of restoring hearing, they can have limitations such as increasing current spread and decreasing frequency resolution due to tissue growth around the electrode array. Impedance measurements in cochlear implants have become a versatile tool for intra- and post-operative diagnosis of cochlear implant state. However, most clinical devices use current pulse stimulation already available in the implants and analyze the voltage response in the time-domain and spread along the cochlea. To use the full potential of impedance spectroscopy in differentiating cell types, measurement over an extended frequency range is required. This study presents a simple electrical equivalent circuit for impedance spectroscopy with cochlear implants in a 2-pole configuration. The electrical equivalent circuit describes the electrical properties of the cochlear implant electrode and its electrochemical behavior at the electrode-electrolyte interface by comparing two non-linear bilayer models, Cole-Cole and Schwan-Faraday. The model is validated for four cochlear implant electrodes from four different manufacturers (MED-EL FlexSoft, AB HiFocus SlimJ, Oticon EVO, Cochlear Nucleus CI622) characterized by impedance spectroscopy between 5 Hz and 13 MHz. In the future, this electrical equivalent circuit may help to extract parameters for differentiating cell types around the cochlear implant electrode from an impedance spectroscopic measurement.

1. Introduction

According to an estimate of the World Health Organization (WHO) currently more than 700 million people suffer from disabling hearing loss worldwide [1,2]. In profound deaf patients, cochlear implants (CI) are an established method to restore hearing by electrically stimulating the spiral ganglion cells in the inner ear. These neuro-implants successfully allow speech recognition in adults and children and more than 800.000 patients were implanted worldwide in 2020 [3]. However, CIs have major technical limitations such as insufficient speech intelligibility in noisy environments and limited frequency resolution. Additionally, pathological processes as osseous and fibrotic tissue growth around the electrode array in the inner ear may increase current spread, decreasing frequency resolution and patient benefit further [4]. As many of the possible sources for variability and limited patient benefit are unknown, diagnostic methods to improve device fitting and to give an

insight into the local status of the cochlea intra- and post-operatively are desirable. Current available methods mainly include the recording of acoustically [5] and electrically evoked potentials [6] and the measurement of electrode impedances.

The latter, initially were intended to test device integrity, but have developed to a versatile tool for intra-operative [7,8] and post-operative [9,10] diagnosis of the cochlear implant state. Clinically used devices today are mostly restricted to simple rectangular constant current stimuli, covering only a limited frequency range. The clinically used impedance is usually derived from the voltage measured at a fixed time during the rectangular current pulse. This basic gross impedance magnitude, averaging across frequencies contained in the rectangular stimulus and the electrical environment of the electrode array, already serves multiple diagnostic purposes, such as e.g. the intra-operative detection of tip-fold-overs with transimpedance matrices (TIM, [11, 12]), determination of full insertion [13] and electrode array position

^{*} Corresponding author.

E-mail addresses: sehlmeyer@geml.uni-hannover.de (M. Sehlmeyer), bhavsar.mit@mh-hannover.de (M.B. Bhavsar), zimmermann@geml.uni-hannover.de (S. Zimmermann), maier.hannes@mh-hannover.de (H. Maier).

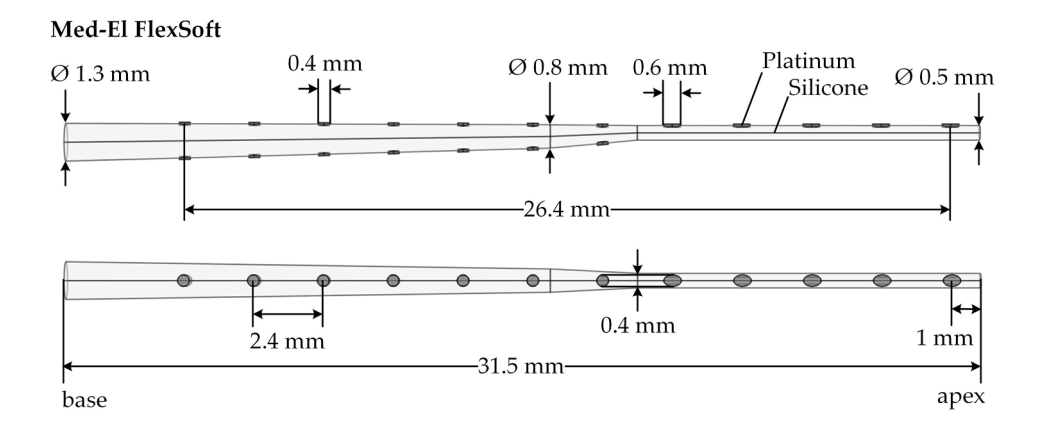
[#] M.S. and M.B.B. equally contributed to this work

M. Sehlmeyer et al. Hearing Research 453 (2024) 109125

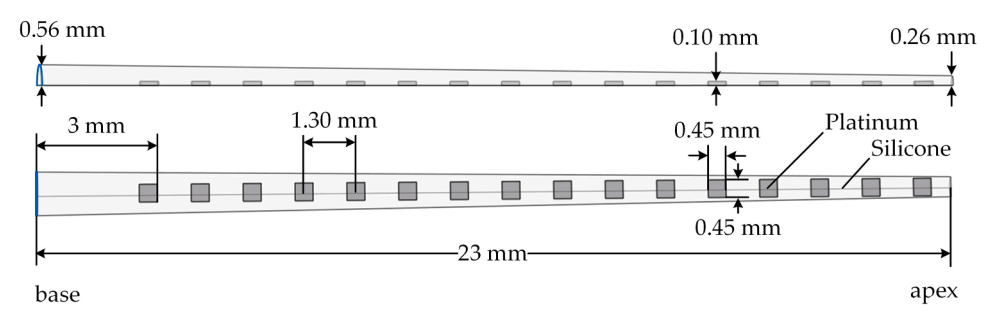
[14].

Impedance spectroscopy over an extended frequency range is used for the detailed analysis of tissue properties and distinction of different cell types [15]. However, to resolve the impedance of the investigated tissue requires proper description of the connecting electric circuit in electrical terms in order to extract the tissue properties. In cochlear implant electrode arrays the impedance, measured at the implant is dominated by the array, the long connection lines, their internal configuration, the bilayer at the platinum/perilymph interface and the return pathway. The usual approach to measure the impedance between one of the electrodes and an extra-cochlear reference electrode has the

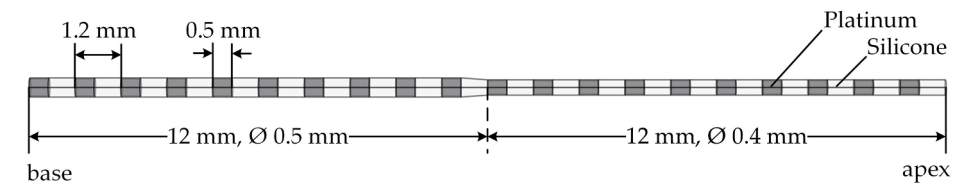
disadvantage that the return pathway and the reference electrode impedance is unknown. Although, in many cases the reference electrode impedance can be assumed to be low enough to be neglected, the return pathway constitutes an underdetermined system [12,16]. Here, finite element models of the cochlear and tissue geometry can give an understanding of the current pathways [16–18], but assumptions of the electrical properties have to be made that decrease the accuracy of the impedance measurement at the site of interest close to the electrodes, inside the cochlea. Three-pole impedance measurement configuration provide a valuable tool to investigate single electrode bilayer impedances, but usually take no connection lines into account and are difficult



Advanced Bionics HiFocus SlimJ



Oticon Medical EVO



Cochlear Nucleus CI622

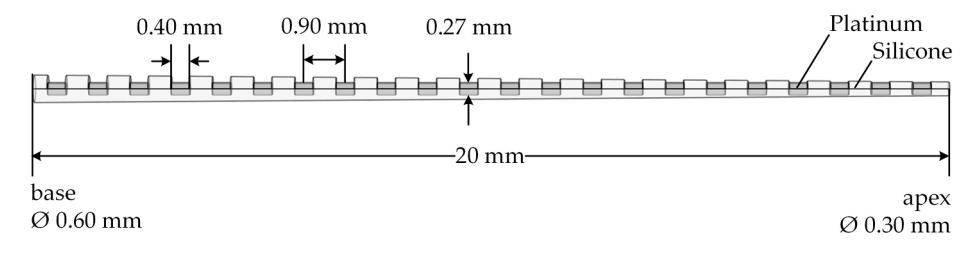


Fig. 1. Geometries of the investigated CI arrays of MED-EL FlexSoft, Advanced Bionics HiFocus SlimJ, Oticon EVO and Cochlear Nucleus CI622 used in FEM simulation. The Pt-stimulation electrodes are embedded in a silicone carrier.

to be implemented in intra-cochlear arrays [19]. Four-pole impedance measurement configurations, that use a constant current stimulus between two outer electrodes of unknown impedance, while measuring the voltage across two high impedance inner electrodes, promise a better defined current pathway in the vicinity of the array and thus local resolution of impedances close to the electrodes [20]. However, precise measurements in this configuration still require knowledge of the current density in the inner electrodes measuring the voltage and the actual current will also depend on the crosstalk, i.e. the capacitance between the connection lines of the current-supplying outer electrodes. Another possibility is to electrically characterize a two-pole (2-pole) configuration in advance and compensate for it in later measurements. Although this alternative approach does not separate the current pathway from the voltage sensing, it provides several advantages such as a very small sensitive volume, simple circuitry with less electrodes involved and the independence of the long-range return pathway.

In the study presented here, we intended a bottom-up approach by first generating and validating an electrical equivalent circuit (EEC) model of the electrical properties of two adjacent electrodes of the array in a 2-pole configuration in a defined electrolytic environment. For the non-linear bilayer in the EEC two physico-chemical models from Cole-Cole and Schwan-Faraday were compared with each other regarding their accuracy and suitability to describe actual measurement result.

Finally, four CIs from four different manufacturers: MED-EL FlexSoft, Advanced Bionics HiFocus SlimJ, Oticon EVO and Cochlear Nucleus CI622 were investigated by impedance spectroscopy. The model was validated for all types and their electrical behavior was analyzed and compared.

2. Materials and methods

The cochlear implant electrodes utilized in this study were provided by four distinct device manufacturers: MED-EL Medical Electronics GmbH (MED-EL, Innsbruck, Austria), Advanced Bionics LLC (AB, Valencia, CA, USA), Oticon Medical/Neurelec SAS (Oticon, Vallauris, France) and Cochlear Ltd. (Cochlear, Sydney, Australia). The cochlear implant electrodes came either with an electrical adapter or were connected by a small custom-made printed circuit board (PCB) for reproducible connection.

Each CI electrode consists of a cable and an electrode array that carries the intra-cochlear stimulation electrodes (SEs). Depending on the manufacturer and model, electrode arrays have different numbers of platinum (Pt) SEs of different shape and size embedded into silicone carriers with different geometry as depicted in Fig. 1.

Each SE is connected to the implant by a fine wire typically made of platinum or platinum-iridium as a connection line. Just like the dimensions of the electrode array, the arrangement of the wires in the silicone carrier of the cable which lead to the SEs and their cross section,

also vary between the different manufacturers (Fig. 2).

Table 1 provides an overview of the specific design parameters associated with each CI electrode regarding stimulation electrodes and wires that were investigated in our study. The SEs are numbered throughout the text in ascending order from the apex (SE1) to the base (Fig. 1).

2.1. Impedance measurement

For all four CI electrodes the complex impedance between two neighboring SEs was measured with an impedance analyzer (HP4192A, Hewlett-Packard Ltd., now: Agilent Technologies Inc., Santa Clara, CA, USA). Prior to measurement, all CI electrodes were cleaned by rinsing them in a solution of enzyme-active detergent Tergazyme® (cat. No. 1304-1, Lot MKCM5800, Alconox Critical Cleaning Experts, New York, USA) for 15 min to remove possible deposits present on the electrodes. Afterwards, all surfaces of the CI electrodes were cleaned by placing them in distilled water for 5 min. A test fixture (16,047, Hewlett-Packard Ltd., now: Agilent Technologies Inc., Santa Clara, CA, USA) was used to connect the CI electrodes to the impedance analyzer. The CI electrodes (MED-EL FlexSoft, AB HiFocus SlimJ, Oticon EVO, Cochlear Nucleus CI622) were placed in a linear cochlea phantom (inner ø 1.2 mm, height 25 mm) in a cylinder made of epoxy (outer ø 25 mm, height 35 mm) filled with artificial perilymph (supplementary information Table S1) [28]. The impedance analyzer was calibrated performing a short and open measurement at the end of the test fixture as described in the impedance analyzer's manual [29]. After calibration, the impedance spectroscopy was performed between all neighboring pairs of stimulation electrodes at logarithmic frequencies (20 points per decade) from 5 Hz to 13 MHz with an amplitude of 100 mV $_{rms}$ without external DC bias voltage using 4192A Sweep Utility software from Kelzenberg [30] at room temperature.

2.2. Electrical equivalent circuit

Electrically a cochlear implant electrode can be divided into three parts as shown in Fig. 3— the wires to the SEs inside the silicone carrier of the cable and the electrode array (green), the bilayer of the SEs and the electrolyte (orange) and the electrolytic medium between two SEs (blue).

In the simplest case the wires can be modeled by an electrical resistance 2 $R_{\rm wa}$ and 2 $R_{\rm wb}$ that is split into a T-circuit for symmetry reasons with a capacitance $C_{\rm ab}$ formed between two active connecting wires inside the silicone carrier. The SEs of a cochlear implant are inert metallic contacts in contact to the perilymph, an electrolyte, in the scala tympani of the inner ear that form a bilayer at the electrode-electrolyte interface [31]. Below the Maxwell-Wagner frequency, the electrolyte between the SEs is modeled by a resistance $R_{\rm m}$ and a capacitance $C_{\rm m}$.

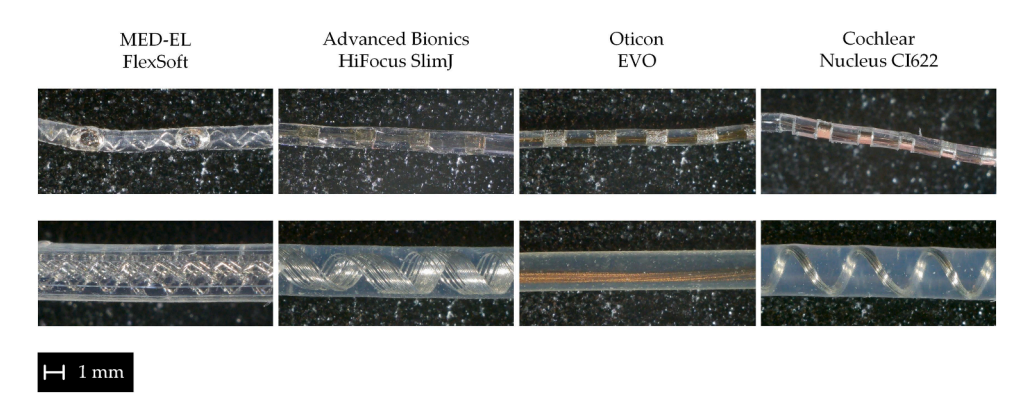
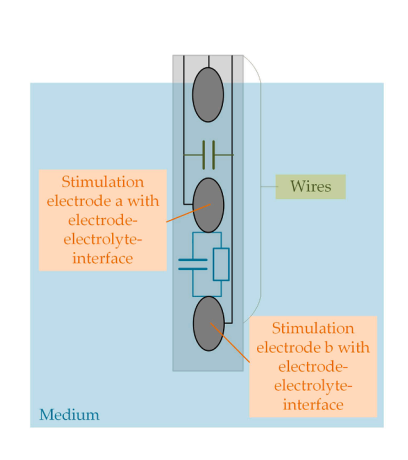


Fig. 2. Internal structures of the four cochlear implant arrays, showing the shape of SEs and connections in between (upper row) and wire arrangement in the cable part (bottom row). The length scaling for both rows is given on the left.

Table 1Overview of investigated cochlear implant electrode arrays with their specifications regarding wires and stimulation electrodes.

CI	Manufacturer	MED-EL [21,22]	Advanced Bionics [23]	Oticon [24,25]	Cochlear [26,27]
	Model	FlexSoft	HiFocus ™ SlimJ	EVO	Nucleus CI622
Stimulation electrodes	Number SEs	12	16	20	22
(SEs)	Active SE area [mm ²]	0.09 (either split or single contacts)	Minimum 0.12	0.46 to 0.60	0.14 to 0.20
	Distance between two neighboring SEs [mm]	2.40	1.30	1.20	0.90
	Total length of electrode array [mm]	31.50	20	24	19.1
	SE shape	Ellipsoid/ spherical	Flattened rectangular	Cylindrical	Partial cylindrical/ recessed
	Silicone carrier shape	Conical/cylinder	Conical/semi- cylinder	Cylinder/ stepped	Conical/cylinder
	Defect SEs	2	None	12; 14; 20	1; 5
Wires	Material	Platinum	Platinum-Iridium	Platinum- Iridium	Platinum-Iridium
	Arrangement	Zig zag	Spiral	Straight	Spiral
	Effective length of the silicone carrier of the cable without SE [mm]	100.00	80.00	190.00	110.00



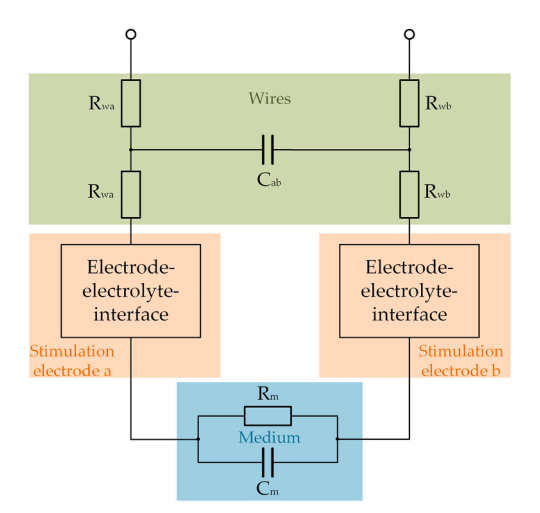


Fig. 3. Left: Schematic depiction of a cochlear implant in electrolyte. Right: Hypothetical electrical equivalent circuit of two SEs a and b of a cochlear implant. The equivalent circuit consists of the connecting wires inside the silicone carrier (green, wire resistances $R_{\rm wa}$, $R_{\rm wb}$ and capacitance between wires $C_{\rm ab}$), the Pt-electrode-electrolyte interfaces (orange) and the electrolyte between the Pt-SEs (blue, resistance $R_{\rm m}$ parallel to capacitance $C_{\rm m}$). $R_{\rm m}$ and $C_{\rm m}$ also account for surrounding tissue depending on the current distribution. However, due to the higher permittivity and conductivity of artificial perilymph compared to the surrounding epoxy cylinder, $R_{\rm m}$ and $C_{\rm m}$ are dominated by the artificial perilymph in this work.

2.3. Characterization of the wire resistance

Each SE has an own wire that connects the SE with the implant. First, each SE combination was measured in air as an open circuit measurement to determine the capacitance C_{ab} (Fig. 3) between the connecting wires. In this case, the capacitance in air between SEs could be neglected as demonstrated by FEM analysis in 3.2. Nevertheless, the model shown in Fig. 3 is an underdetermined system with more undefined variables than boundary conditions and the resistances arising from the connecting wires have to be measured independently. Therefore, a device to contact the electrodes with a Pt-wire contact was built (Fig. 4) and the resistance of each electrode with its connecting wire was measured independently to determine R_{wa} and R_{wb} (Fig. 3).

2.4. Bilayer models for the electrode-electrolyte interface

The electrode-electrolyte interface has already been described by different models. Here, we investigated two different models for the bilayer, described by Cole-Cole [32–34] and Schwan-Faraday [35–38]. Both bilayer models investigated are summarized in Table 2.

Platinum is probably the best investigated polarizable electrode example. For such electrodes in electrolyte, the bilayer shows a pro-

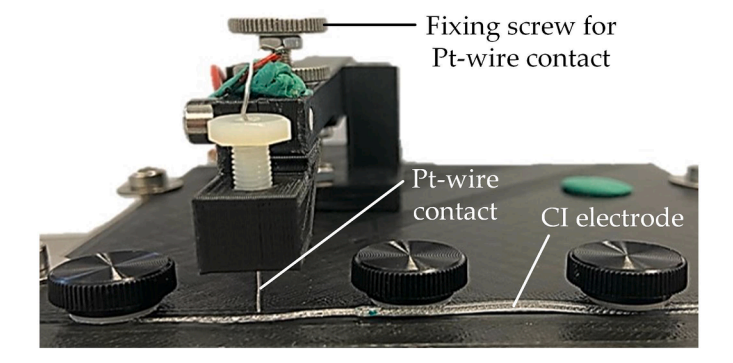
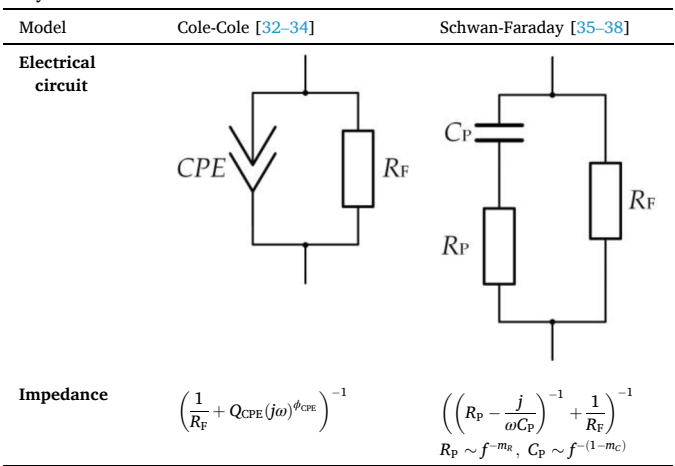


Fig. 4. Measuring setup for determining the individual wire resistances inside a CI.

nounced non-linear behavior [33,36]. Schwan et al. described the bilayer as a frequency-dependent polarization capacitance C_P in series with a frequency-dependent polarization resistance R_P which results in a constant phase (Table 2) [35,38]. Cole and Cole described the bilayer as a later called constant phase element (CPE) shown in Table 2 [32–34].

Table 2 Bilayer models from literature.



The CPE models the impedance arising from the electrolytic double layer capacitance at the electrode surface. Unlike an ideal capacitor, which has a -90° delay, the CPE exhibits a constant phase shift that deviates from this ideal behavior. This characteristic makes the CPE a non-ideal non-linear capacitor [39]. It consists of a capacitance parameter Q_{CPE} and a CPE exponent $-1 \leq \phi_{\text{CPE}} \leq 1$ [33,40]. Both models are in parallel to a frequency-independent Faraday resistance R_{F} to describe electrochemical reactions at the electrode-electrolyte interface [33].

The parameters for the Cole-Cole bilayer model were calculated from the measured impedance magnitude $|\underline{Z}|$ and the phase angle φ (Fig. 5 left). To determine the CPE exponent ϕ_{CPE} , the impedance magnitude was fitted with a linear regression between 5 Hz and 1 kHz. Knowing ϕ_{CPE} , the bilayer capacitance parameter Q_{CPE} was calculated from the impedance magnitude at the frequency where the phase angle is minimal because there the CI behavior is mostly capacitive (purely capacitive behavior: $\varphi=-90^{\circ}$).

For the Schwan-Faraday bilayer model, the parameters were calculated from the real part $Re(\underline{Z})$ and imaginary part $Im(\underline{Z})$ of the impedance measurements (Fig. 5 right). The polarization capacitance C_P has the highest impact on the imaginary part of the bilayer impedance.

Therefore, the imaginary part was fitted by a linear regression between 5 Hz and 10 kHz. The gradient of the fitting supplied the frequency exponent m_C . C_P was calculated with this gradient in the middle of the fitted frequency range at 200 Hz (Fig. 5 right, blue markers). The parameters for the polarization resistance R_P and m_R were determined the same way in a frequency range between 5 Hz and 1 kHz from the linear section of the real part (Fig. 5 right, red markers). The frequency dependence applied to the polarization components can be found in Table 2.

The parallel resistance $R_{\rm F}$ was calculated from the complex impedance at the lowest measured frequency of 5 Hz for both models. The capacitances $C_{\rm ab}$ and $C_{\rm m}$ were assumed to have an infinite impedance at 5 Hz and thus to behave like open circuits (Fig. 3 right). Therefore, the sum of $R_{\rm m}$, 2 $R_{\rm wa}$ and 2 $R_{\rm wb}$ could be subtracted from the measured complex impedance at 5 Hz. By resolving the parallel bilayer circuit, the Faraday resistance $R_{\rm F}$ was then obtained from the previously calculated bilayer parameters of the polarization path and the complex impedance at 5 Hz.

The EECs were evaluated using an error calculation as a measure of how well the modelled values for complex impedance $\underline{Z}_{\mathrm{mod}}$, magnitude $|\underline{Z}|_{\mathrm{mod}}$ and phase angle φ_{mod} represent the measured complex impedance $\underline{Z}_{\mathrm{meas}}$, magnitude $|\underline{Z}|_{\mathrm{meas}}$ and phase angle φ_{meas} . Therefore, the absolute error e_{φ} for phase angle and the relative errors e_{Z} for magnitude and e_{Z} for complex impedance were calculated for each neighboring SE combination for all frequencies f_{i} with i=1,...N. For those errors, the arithmetic means \overline{e}_{φ} , \overline{e}_{Z} and \overline{e}_{logZ} across all frequencies (eq. (1) to (3)) and their standard deviations σ_{φ} , σ_{Z} and σ_{Z} were calculated.

$$\bar{e}_{\varphi} = \frac{1}{N} \sum_{i=1}^{N} |\varphi_{\text{mod}}(f_i) - \varphi_{\text{meas}}(f_i)| \tag{1}$$

$$\overline{e}_{Z} = \frac{1}{N} \sum_{i=1}^{N} \frac{\left| \left| \underline{Z}_{\text{mod}}(f_{i}) \right| - \left| \underline{Z}_{\text{meas}}(f_{i}) \right| \right|}{\left| \underline{Z}_{\text{meas}}(f_{i}) \right|}$$
(2)

$$\bar{e}_{\underline{Z}} = \frac{1}{N} \sum_{i=1}^{N} \frac{\left| \underline{Z}_{\text{mod}}(f_i) - \underline{Z}_{\text{meas}}(f_i) \right|}{\left| \underline{Z}_{\text{meas}}(f_i) \right|}$$
(3)

Additionally, the arithmetic means $\overline{\overline{e_w}}$, $\overline{\overline{e_z}}$ and $\overline{\overline{e_z}}$ and standard

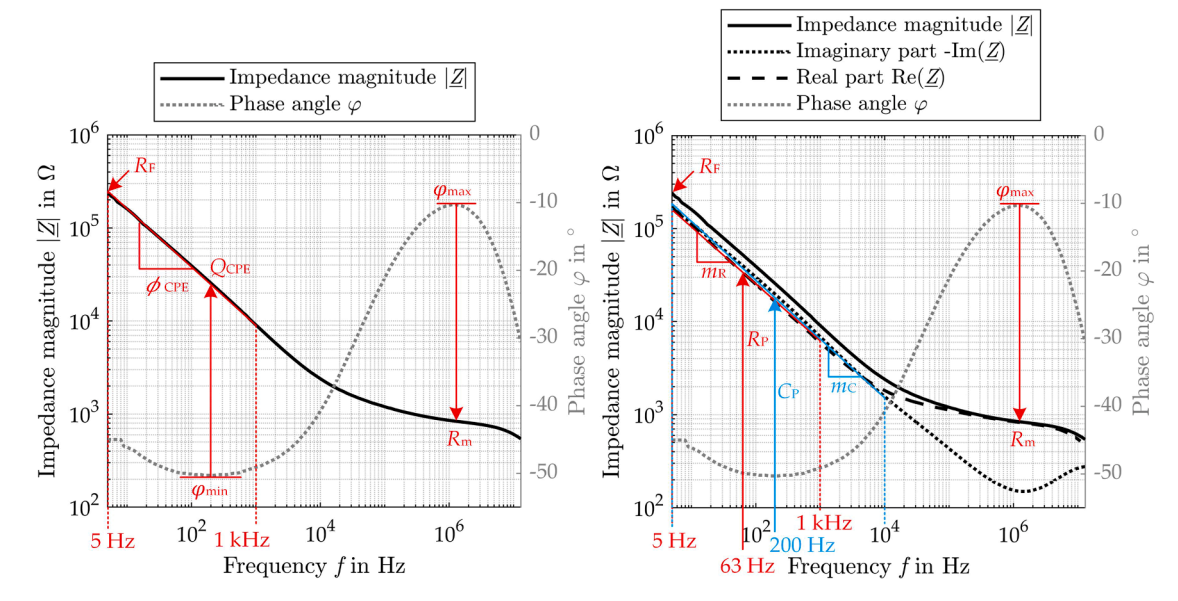


Fig. 5. Exemplary impedance measurement between the two most apical SEs of the Oticon EVO electrode. Left: Determination of Cole-Cole parameters from an impedance measurement analyzing the impedance magnitude $|\underline{Z}|$ and the phase angle φ . Right: Determination of Schwan-Faraday parameters from an impedance measurement analyzing the real part $Re(\underline{Z})$ and the imaginary part $Im(\underline{Z})$. The diagram shows the negative imaginary part.

deviations $\sigma_{\overline{e}\varphi}$, $\sigma_{\overline{e}Z}$ and $\sigma_{\overline{e}\underline{Z}}$ across all neighboring SE combinations were calculated from the averaged errors across all frequencies.

The parameters for the bilayer models were calculated in MATLAB R2023b by analyzing the measurement data as described above without using any further data processing or optimization algorithm.

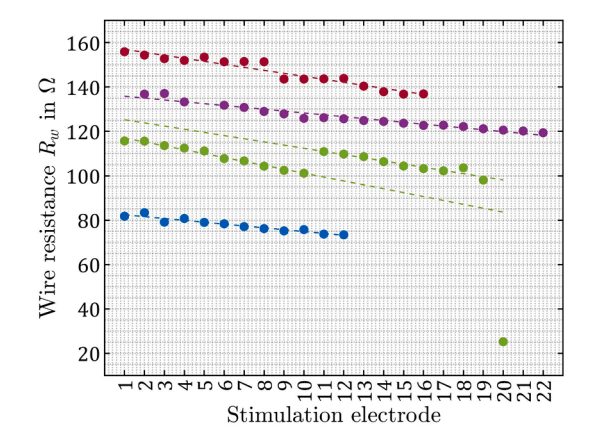
2.5. Characterization of the interaction between SEs and the surrounding medium

In simple terms, two SEs in an electrolyte form a capacitor $C_{\rm m}$ with the electrolyte as the dielectric and a parallel resistance $R_{\rm m}$, where $R_{\rm m}$ also includes the surrounding tissue. However, due to the higher permittivity and conductivity of artificial perilymph compared to the surrounding epoxy, $R_{\rm m}$ and $C_{\rm m}$ are dominated by the electrolyte. The electrolyte resistance $R_{\rm m}$ was for all bilayer models taken from the impedance magnitude at the frequency where the phase angle was maximal minus the sum of the wire resistances $2\,R_{\rm wa}$ and $2\,R_{\rm wb}$ as shown in Fig. 5. At this frequency, the CI behaves mostly resistive (purely resistive behavior: φ =0) and the bilayer can be assumed as nearly short circuited by its polarization path. However, to consider a possible residual bilayer contribution at this frequency $R_{\rm m}$ was corrected further by subtracting the real part of the calculated bilayer impedances.

In order to determine the capacitance, electrostatic FEM simulations in Comsol Multiphysics were carried out for all investigated CI geometries (Fig. 1). In the simulation, one of the two SEs under consideration had a potential of 50 mV, while the second SE had a potential of -50 mV. The geometry of the FEM simulation models for the four investigated CI electrode types were taken as depicted in Fig. 1. For the electrode carrier, polydimethylsiloxane (PDMS) with a relative permittivity of ε_r 2.69 [41] was used and the stimulation Pt-electrodes were assumed as perfect electric conductors in the model. In the simulation, the CI electrodes were placed in the middle of a cylindrical hole of 0.9 mm radius and a length of 26 mm filled with saline ($\varepsilon_r = 80.21$ at 20 °C [42]) in an epoxy cylinder. The epoxy cylinder with $\varepsilon_r=3.50$ [21] had an outer radius of 7 mm and a length of 30 mm. The capacitance was calculated by dividing the charge on the positive charged SE by the potential difference. Additionally, the CI electrode was simulated in the middle of an air cylinder with $\epsilon_r=1\text{, a radius of 20 mm}$ and a length of 60 mm.

3. Results

In order to determine the EEC of the four CI electrodes investigated, differences in their design and impedance spectroscopic measurements were analyzed. As the model in Fig. 3 constitutes an under-determined system, firstly elements $R_{\rm wa}$, $R_{\rm wb}$, $C_{\rm ab}$ were determined separately. The bilayer properties $Q_{\rm CPE}$, $\varphi_{\rm CPE}$, $R_{\rm P}$, $C_{\rm P}$, m_R , m_C and the medium properties



 $R_{\rm m}$, $C_{\rm m}$ were calculated afterwards by two different bilayer models.

3.1. Connecting wire properties: resistances and capacitances

Fig. 6 left shows the measured resistances (raw data) to each SE of the investigated CIs measured with a Pt-wire contact. The relationship between the resistance of the wires and the distance of the SE from the connector at the basal end was directly proportional and could be fitted linear. The Oticon electrode showed an exceptional resistance step in the raw measurements between SE10 and SE11. The reason were different lead lengths at the rear connector resulting in SE1 and SE11 having the longest leads inside the connector and SE10 and SE20 the shortest. A further exception was the most basal contact SE20 that had a significantly larger wire diameter of 50 μm than the other wires with 25 μm (personal communication: Oticon Medical). Normalization of the measured resistance to the silicone carrier length and the length of leads in the connector resulted in nearly constant estimated resistance per effective length (Fig. 6 right and supplementary information Figure S1) with averages of 5.15 \pm 0.08 Ω /cm for Oticon EVO, 6.35 \pm 0.12 Ω /cm for MED-EL FlexSoft, 7.94 \pm 0.09 Ω /cm for Cochlear Nucleus CI622 and $16.30 \pm 0.44 \,\Omega/cm$ for AB HiFocus SlimJ. The slopes of the linear fit provide the following resistances between two neighboring SEs: 0.84 Ω for MED-EL FlexSoft, 1.35 Ω for AB HiFocus SlimJ, 1.76 Ω apical and $1.43~\Omega$ basal for Oticon EVO (SE20 excluded) and $0.84~\Omega$ for Cochlear Nucleus CI622.

3.2. Capacitance between stimulation electrodes

The measured capacitances between neighboring electrode pairs measured in air ranged from 7.46 pF to 20.36 pF across all four CI electrodes. Although a trend towards smaller capacitances with increasing spacing could be observed, the results were far less systematic than for wire resistances (Fig. 7 left). Normalization of the measured capacitances to the silicone carrier length and the length of leads in the connector resulted in capacitances per effective length between 0.50 \pm 0.09 pF/cm for Oticon EVO and 1.31 \pm 0.14 pF/cm for AB HiFocus SlimJ (Fig. 7 right, supplementary information Figure S2).

For segregation of the wire from the SE contributions, the capacitances between two SEs were determined by FEM simulation of the geometries shown in Fig. 1 in air, resulting in values between $16.03~\rm fF$ and $27.53~\rm fF$ (Fig. 8 left). As the results from the simulation amount to maximally $0.37~\rm \%$ of the total measured wire capacitance of the array for neighboring SEs, the medium capacitance can be assumed as negligible in the air measurements. The capacitances determined by FEM simulation in a linear volume filled with the electrolyte between the SEs resulted in values between $0.35~\rm pF$ for Cochlear and $1.07~\rm pF$ for Oticon.

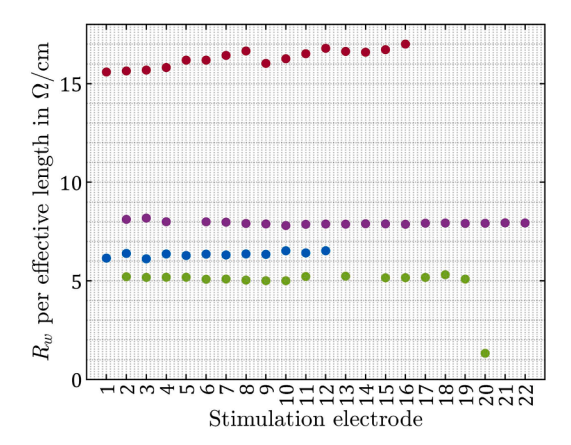


Fig. 6. Left: Measured wire resistances of the investigated cochlear implants MED-EL FlexSoft (blue), AB HiFocus SlimJ (red), Oticon EVO (green) and Cochlear Nucleus CI622 (purple). The resistance of the most basal contact (SE20) from Oticon EVO was significant lower due to a larger diameter. Right: Normalized wire resistances to the length of electrode array and associated connector (effective length).

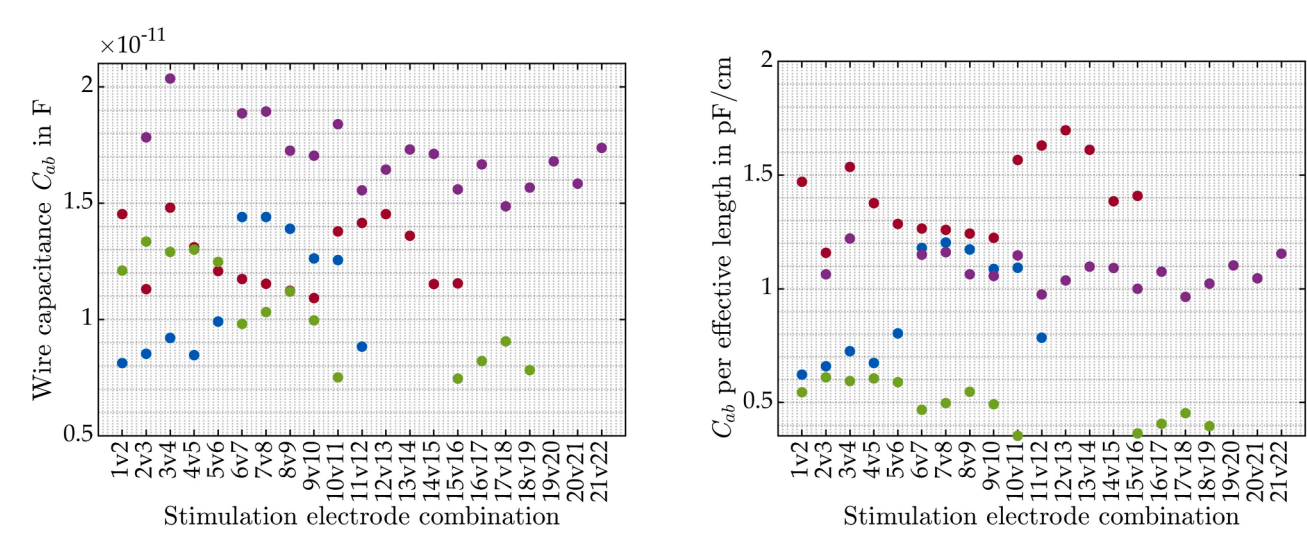


Fig. 7. Left: Measured wire capacitances of the investigated cochlear implants MED-EL FlexSoft (blue), AB HiFocus SlimJ (red), Oticon EVO (green) and Cochlear Nucleus CI622 (purple). Right: Normalized wire capacitances to the length of electrode array and associated connector.

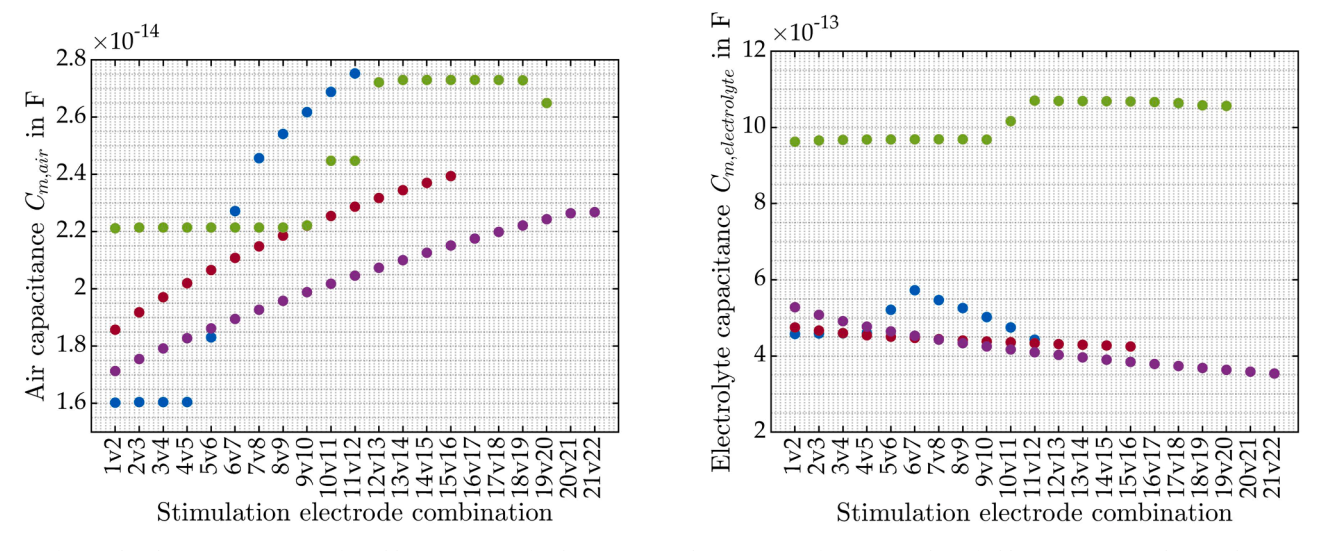


Fig. 8. Left: Simulated capacitances in air of neighboring SE pairs for the geometries shown in Fig. 1 for MED-EL FlexSoft (blue), AB HiFocus SlimJ (red), Oticon EVO (green) and Cochlear Nucleus CI622 (purple). Right: Capacitances in electrolyte of neighboring SE pairs determined by FEM simulation for MED-EL FlexSoft (blue), AB HiFocus SlimJ (red), Oticon EVO (green) and Cochlear Nucleus CI622 (purple).

In contrast, when perilymph instead of air was assumed as the surrounding medium in the FEM simulation (Fig. 8 right), capacitances amounted to a maximum of 14.34 % of the total measured capacitance and were therefore considered in the following calculations.

3.3. Bilayer model parameters

With the findings of the previous sections, the parameters for the two-bilayer models could be calculated including the measured data for $R_{\rm wa}$, $R_{\rm wb}$, $C_{\rm ab}$ and $C_{\rm m}$ into the EEC. The results for the whole EEC are

Table 3Example parameter set for the electrical equivalent circuit with a Cole-Cole bilayer model for the two most apical (functional) identical SEs.

Bilayer parameters		MED-EL FlexSoft (SE3 vs SE4)	Advanced Bionics HiFocus SlimJ (SE1 vs SE2)	Oticon EVO (SE1 vs SE2)	Cochlear Nucleus CI622 (SE2 vs SE3)
Measured/simulated	$R_{\rm wa}$ [Ω]	39.55	77.95	57.85	68.40
parameters	R_{wb} [Ω]	40.38	77.2	57.80	68.55
	C_{ab} [pF]	9.21	14.53	12.10	17.83
	$C_{\rm m}$ [pF]	0.46	0.48	0.96	0.51
Calculated parameters	$R_{\rm m}$ [k Ω]	3.64	3.11	0.54	1.42
	$egin{aligned} Q_{ ext{CPEa}} &= \ Q_{ ext{CPEb}} & [ext{nF}ullet ext{s}^{\Phi ext{-}1}] \end{aligned}$	148.93	141.57	977.20	156.68
	$\phi = \phi_{ extsf{CPEa}} = \phi_{ extsf{CPEb}}$ [-]	0.81	0.77	0.61	0.82
	$R_{\mathrm{Fa}} = R_{\mathrm{Fb}} [\mathrm{M}\Omega]$	5.50	20.20	0.68	4.67

summarized in the following two sections for the Cole-Cole bilayer model and the Schwan-Faraday bilayer model. In both cases, the two active SEs and their electrode-electrolyte interface were assumed identical.

3.3.1. Cole-Cole

As an example, the calculated parameters of the two most apical intact, neighboring SEs with a Cole-Cole bilayer model for all investigated CI types are summarized in Table 3.

The correspondence between the measured and calculated impedances from the model with the respective parameter sets from Table 3 are shown in Fig. 9. For each implant the most apical intact SE combination is depicted as an example.

Table 4 summarizes the averaged relative errors over the whole frequency spectrum between the calculated complex impedance, magnitude and phase angle related to the measurements for the most apical SE combination and as an average over all neighboring SE combinations for all four implants.

3.3.2. Schwan-Faraday

Table 5 summarizes the calculated values for the Schwan-Faraday bilayer parameters for the most apical intact, neighboring SE combination of the four CI electrodes.

Fig. 10 shows the correspondence between the measurement data and the calculated complex impedance \underline{Z} , magnitude $|\underline{Z}|$ as well as the calculated phase angle φ with the EEC in Fig. 3 including a Schwan-Faraday bilayer model and the calculated parameter values in Table 5.

The averaged relative errors over the whole frequency spectrum between the calculated complex impedance, magnitude and phase angle related to the measurements for the most apical SE combination and as an average across all neighboring SE combinations for all four implants are summarized in Table 6.

4. Discussion

In this study we developed an electrical equivalent circuit (EEC) to describe the basic electric properties of cochlear implant electrode arrays when employed in a 2-pole configuration for high resolution impedance spectroscopy. The model is based on linear elements to describe the properties of the array in combination with two common non-linear electrochemical bilayer models, the Cole-Cole and the Schwan-Faraday model, of the electrode-electrolyte interface. As even the simple model constitutes an underdetermined system, measurements and FEM simulations were carried out to determine the lacking electrical parameters of four exemplary commercial CI electrode arrays (MED-EL FlexSoft, AB HiFocus SlimJ, Oticon EVO, Cochlear Nucleus CI622). The model was applied to measurement data of the array in a simple cylindrical geometry filled with artificial perilymph and the accuracy of the model was determined. An exemplary measurement is shown in Fig. 11 for illustration.

As described in Section 2.2, the CI electrode array was modeled by a simplified EEC consisting of two linear parts – the wires in the silicone CI carrier and the electrolyte – and a non-linear electrode-electrolyte interface describing the bilayer.

At low frequencies, with $C_{ab} < 18$ pF and $R_{wa} < 78$ Ω (Table 3) the capacitive pathway between the wires and with $C_m < 1.1$ pF (Table 3, FEM simulation) and $R_m < 4$ k Ω (Table 3), the capacitance of the medium can be neglected for f < 2 MHz for all electrode arrays. The low frequency impedance is dominated by the bilayer up to ≤ 50 kHz where $|Z_{bilayer}| \geq 2R_{wa} + 2R_{wb} + R_m$ for all investigated electrodes. This estimate justifies the appropriate choice of the frequency range for the determination of parameters of the Cole-Cole and the Schwan-Faraday bilayer model (Fig. 5) in retrospective. Above 50 kHz the measured impedance becomes mainly ohmic, characterized by a maximum in phase angle, although in all measurements a clear ohmic plateau region

was not identifiable.

At high frequencies, the impact of C_{ab} and C_m becomes visible in the measurements. Assuming $R_m < 4~\mathrm{k}\Omega$ and $C_{ab} < 18~\mathrm{pF}$ (Table 3) results in a worst case corner frequency $> 2.2~\mathrm{MHz}$ where a capacitive effect between adjacent electrodes becomes significant in measured impedances (Fig. 11). Although, a first order estimate of independent neighboring electrodes fits quite well our results, electrodes in the array are interconnected by their relative wire capacitances and the respective resistances of the electrolyte. Hence, measurements of all possible pairs of stimulation electrodes lead to lower corner frequencies specifically for more distant electrode pairs (see Fig. 12).

As a consequence of the narrow gap between the frequency limits, a clear plateau where the resistance dominates was not identifiable in all measurements. Nevertheless, a clear separation into three frequency ranges dominated by (1) a bilayer impedance, (2) a resistive domain given by the electrolyte and (3) a high frequency region where a significant amount between wires start to contribute to the 2-pole resistance is possible.

Although, the frequency window allowing direct access to the purely resistive pathway between neighboring electrodes is restricted, the resistance of the electrolyte and thus the concentration can be determined with sufficiently high accuracy. Using the average impedance between 50 kHz and 500 kHz even minor changes in the medium can be resolved, such as the impedance change due to the diameter change of the array between SE10/SE11 of the Oticon EVO electrode array (see Fig. 12, right) or the tapering of the AB HiFocus SlimJ, MED-EL FlexSoft or Cochlear Nucleus CI622 electrode arrays (data not shown). The same applies to measurements across more distant SE pairs, although the upper frequency limit is reduced. As can be seen in Fig. 12, the upper corner frequency is substantially shifted to lower frequencies < 10 MHz with increasing SE distance. In cases of more distant SE pairs, as shown by a detailed analysis, the entire network has to be considered, explaining the downshift in corner-frequency and the high-frequency slope < 1 for the logarithmic magnitude (data not shown). However, this effect remains minimal in neighboring electrode pairs (see Fig. 12) and was neglected in our current analysis.

The calculated resistances of the electrolyte from the analysis between neighboring SEs differ between investigated CI arrays and along the length of each array (supplementary information Table S2 and S3). The Oticon EVO had the lowest average medium resistance of $R_{\rm m}=0.51$

 \pm 0.06 $k\Omega$ for Cole-Cole model (0.52 \pm 0.05 $k\Omega$ for Schwan-Faraday model), followed by Cochlear Nucleus CI622 with 1.77 \pm 0.48 k Ω $(1.70\pm0.42\,\mathrm{k}\Omega)$, Advanced Bionics HiFocus SlimJ with $2.00\pm0.33\,\mathrm{k}\Omega$ (1.93 \pm 0.34 kΩ) and MED-EL FlexSoft with 4.75 \pm 1.43 kΩ (4.68 \pm 1.41 k Ω). As the differences in $R_{\rm m}$ between both models were generally small (< 5 %), the medium resistance R_m between two SEs depends on the cross section available for the current, their distance and the electric conductivity of the artificial perilymph, when considering the perilymph dominating the conductivity of the medium/material surrounding the SEs. Estimating $R_{\rm m}$ from the electrolyte filled (~15 S/m) effective cross section, assuming a bore hole of 1.2 mm diameter and deducting the cross section of the isolating silicone carrier of the respective electrode array (see Fig. 1), led to values reflecting the available effective cross section for the electrode in the same order of magnitude, but approximately half the size. However, taking into account that (1) the electrode geometry is far from a parallel plate capacitor configuration, (2) SEs differ significantly in size (Table 1) and (3) that SEs are asymmetrically arranged in the hole, the measured medium resistances $R_{\rm m}$ are therefore in a plausible range. This is also supported by the Oticon design with the largest electrode area covering the entire circumference, resulting in the lowest R_m . A more accurate comparison would have required the exact knowledge of the position and orientation of the electrodes in combination with a FEM model analysis.

MED-EL FlexSoft (SE3 vs SE4)

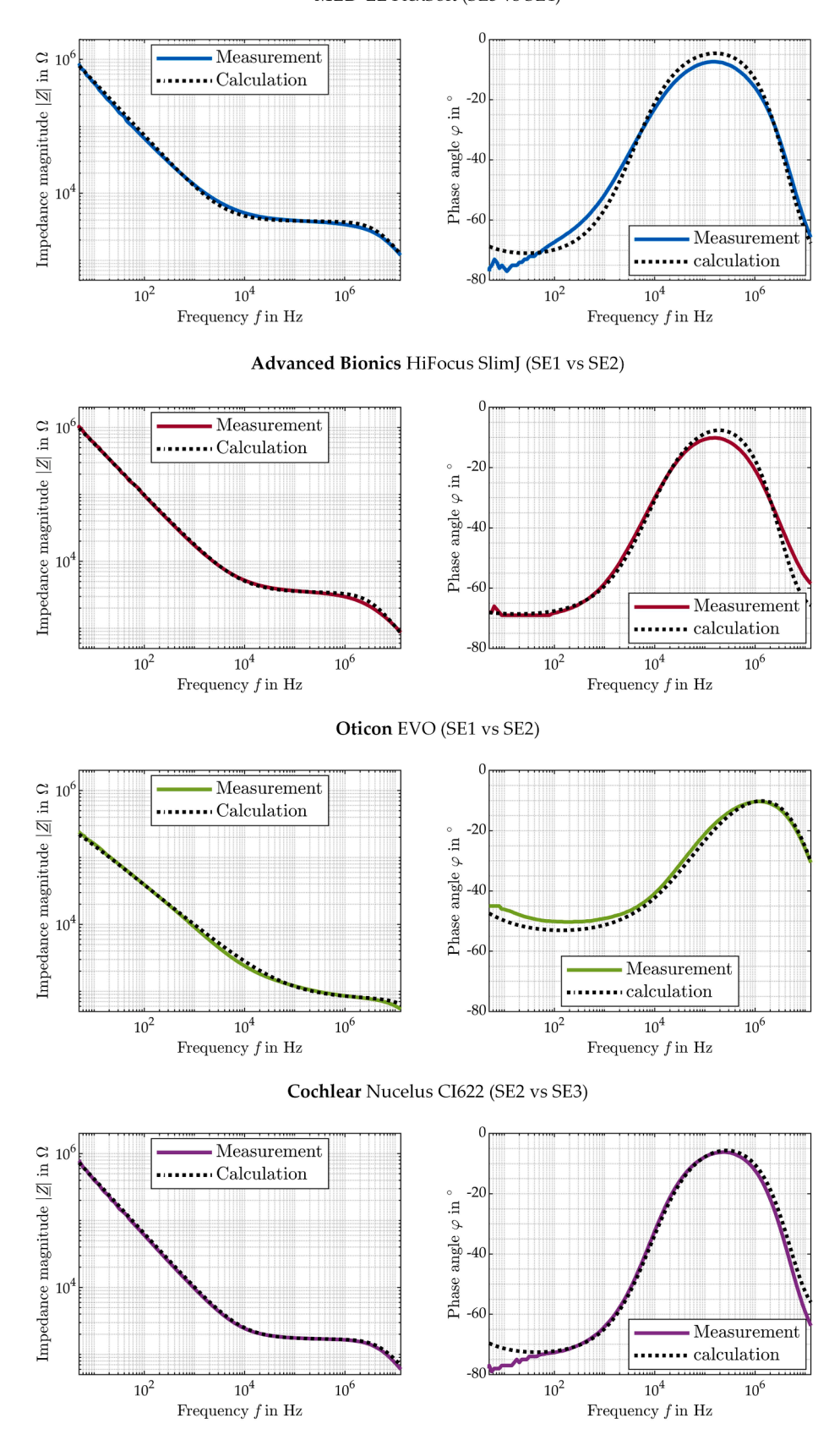


Fig. 9. Correspondence between the calculated (black dotted lines) impedance magnitude $|\underline{Z}|$ and phase angle φ and the measurement data (colored solid lines) for the Cole-Cole bilayer model. As an example, the most apical intact SE combination of the four CI electrodes MED-EL FlexSoft (blue), AB HiFocus SlimJ (red), Oticon EVO (green) and Cochlear Nucleus CI622 (purple) is shown.

Table 4

Average errors across all neighboring SE combinations for the calculation of magnitude, phase angle and complex impedance related to the measured values over the whole frequency spectrum with a Cole-Cole bilayer model.

Errors (average across all frequencies)		MED-EL FlexSoft	Advanced Bionics HiFocus SlimJ	Oticon EVO	Cochlear Nucleus CI622
Most apical SE combination	Magnitude \overline{e}_Z [%]	6.88 ± 3.98	3.82 ± 4.11	6.24 ± 5.99	3.94 ± 3.16
	Phase angle \overline{e}_{φ} [$^{\circ}$]	2.98 ± 1.49	1.85 ± 2.01	1.90 ± 1.04	2.06 ± 2.26
	Complex impedance \overline{e}_Z	9.51 ± 2.65	5.64 ± 4.83	7.82 ± 5.30	5.97 ± 4.42
	[%]				
Average of all neighboring SE	Magnitude $\overline{\overline{e}_Z}$ [%]	8.36 ± 1.08	3.94 ± 1.24	5.88 ± 2.17	5.51 ± 1.92
combinations	Phase angle $\overline{\overline{e}_{\varphi}}$ [$^{\circ}$]	3.69 ± 0.59	1.63 ± 0.58	5.59 ± 3.22	2.22 ± 0.50
	Complex impedance $\overline{\overline{e}_Z}$	11.62 ± 1.43	5.43 ± 1.74	12.81 \pm	$\textbf{7.44} \pm \textbf{2.27}$
	[%]			6.19	

Table 5Exemplary parameter sets for the electrical equivalent circuit with a Schwan-Faraday bilayer model for the two most apical (functional) identical SEs.

Bilayer paramet	ers	MED-EL FlexSoft (SE3 vs SE4)	Advanced Bionics HiFocus SlimJ (SE1 vs SE2)	Oticon EVO (SE1 vs SE2)	Cochlear Nucleus CI622 (SE2 vs SE3)
Measured/	$R_{\rm wa} \ [\Omega]$	39.55	77.95	57.85	68.4
simulated	$R_{\rm wb}$ [Ω]	40.38	77.20	57.80	68.55
parameters	C_{ab} [pF]	9.21	14.53	12.10	17.83
	$C_{\rm m}$ [pF]	0.46	0.48	0.96	0.51
Calculated	$R_{\rm m}$ [k Ω]	3.56	3.04	0.55	1.36
parameters	$C_{Pa} = C_{Pb} [nF]$	123.56	99.04	600.24	121.17
	$egin{aligned} m_{Ca} &= m_{Cb} \ \hbox{[-]} \end{aligned}$	0.81	0.78	0.62	0.83
	$R_{\mathrm{Pa}} = R_{\mathrm{Pb}} \ [\mathrm{k}\Omega]$	261.90	498.67	230.45	224.16
	$egin{aligned} m_{Ra} &= \ m_{Rb} & ext{[-]} \end{aligned}$	0.69	0.72	0.63	0.69
	$R_{\mathrm{Fa}} = R_{\mathrm{Fb}} \ [\mathrm{M}\Omega]$	2.78	9.11	1.21	3.83

4.1. Wire properties

The wire resistances R_{wa} and R_{wb} were measured individually for each SE of every CI electrode with a non-electrolytic metallic contact as they cannot be determined from the impedance measurement in the electrolyte. Although our analysis of effective resistance and capacitance per unit carrier length was performed taking only the length between SE and connector, without distinction between the different sections (connector, wire, electrode array), the wire resistances had 1–3 % standard deviation between different electrodes. Oticon EVO electrodes had the lowest resistance/effective length of 5.15 \pm 0.08 Ω /cm (supplementary information Figure S1), excluding SE20, the most basal electrode that has a significant lower resistance due to a different wire diameter (personal communication: Oticon Medical), followed by MED-EL FlexSoft with 6.35 \pm 0.12 Ω /cm and Cochlear Nucleus CI622 with 7.94 \pm 0.09 Ω /cm resistance/effective length. AB HiFocus SlimJ showed the highest resistance/effective length of 16.30 \pm 0.44 Ω /cm.

In contrast to resistance the capacitance per unit length was less predictable by the effective length with 6–26 % standard deviation. As for resistances, Oticon EVO electrode had the smallest capacitance/per effective length of 0.50 \pm 0.09 pF/cm (supplementary information Figure S2), followed by MED-EL FlexSoft (0.91 \pm 0.24 pF/cm), Cochlear Nucleus CI622 (1.08 \pm 0.07 pF/cm) and AB HiFocus SlimJ (1.31 \pm 0.14 pF/cm). Interestingly, a lower wire capacitance was seen in the case of 11v12 and 1v2 – 5v6 for the MED-EL FlexSoft array. This could be due to inherent variability (arising from its construction or material) or the different geometry of the electrodes symmetrically on both sides at the basal end or on one side at the apex. However, the latter argument does not apply for the most basal electrode (11v12) and the lower

capacitance remains somehow unexplained.

The configuration of leads in the silicone carrier is usually determined by more factors than electrical alone, such as mechanical properties during handling, insertion or manufacturing. From an electrical viewpoint straight wire bundles (Oticon) minimize resistance and capacitance for a given carrier length and a zigzag design (MED-EL) to a lesser extent, whereas a coiled bundle design (AB, Cochlear) results in higher wire resistance and capacitive crosstalk between the connection wires. In contrast to the wire resistance that is accurately predictable from the geometry and the carrier length, capacitances between pairs are highly variable, especially for the zigzag design and probably depend more on arbitrary distribution in the bundle and silicone carrier.

4.2. Bilayer models

For the **Cole-Cole model** example, the bilayer capacitance parameters $Q_{\rm CPEa}$ and $Q_{\rm CPEb}$ are between 141.47 nF s^{-0.23} for AB HiFocus SlimJ and 977.20 nF s^{-0.39} for Oticon EVO (Table 3). For an electrolyte concentration of 0.15 mol/l artificial perilymph, the Debye length can be assumed as ~1 nm [36] and the relative permittivity of artificial perilymph can be estimated for low concentrations as ~80. Assuming a linear capacitance of the bilayer with a distance of the Debye length, results in case of the Oticon EVO example (Table 1, 0.46 mm²) in 325.83 nF being in the range of Cole-Cole model results at low frequencies.

The Faraday resistances $R_{\rm Fa}$ and $R_{\rm Fb}$ in the example are 0.68 M Ω for Oticon EVO, 4.67 M Ω for Cochlear Nucleus CI622, 5.50 M Ω for MED-EL FlexSoft and 20.20 M Ω for Advanced Bionics HiFocus SlimJ (Table 3), being roughly inverse to the SE areas, except for MED-EL. The statistical distribution shows a pronounced variability (supplementary information Table S2 and S3). This may have its origin in the fact that the low frequency limit is not reached at our lowest investigated frequency, resulting in reduced accuracy in $R_{\rm Fa}$ and $R_{\rm Fb}$.

The parameters for the **Schwan-Faraday model** also differ between the investigated CI electrodes. The derived medium resistances $R_{\rm m}$ were similar for both models (Table 5). The calculated values for the polarization capacitances $C_{\rm Pa}$ and $C_{\rm Pb}$ (with a frequency exponent $m_C < 1$) were in the same range as the bilayer capacitance parameters $Q_{\rm CPEa}$ and $Q_{\rm CPEb}$ in the Cole-Cole model, ranging from 99.04 to 600.24 nF. The polarization resistances $R_{\rm Pa}$ and $R_{\rm Pb}$ were smaller ranging from 224.16 k Ω (Cochlear Nucleus CI622) to 498.67 k Ω (AB HiFocus SlimJ).

When comparing the accuracy of the two models to the measured data deviation of the complex impedance \underline{Z} according to (eq. (3)), errors across all neighboring electrodes ranged between 5.43 \pm 1.74 % (AB HiFocus SlimJ) to 12.81 \pm 6.19 % (Oticon EVO) for the Cole-Cole approach and between 6.03 \pm 1.78 % for AB HiFocus SlimJ and 10.41

\pm 1.26 % for MED-EL FlexSoft for the Schwan-Faraday approach.

Average errors in magnitude alone (eq. (1)) were between 3.94 \pm 1.24 % (AB HiFocus SlimJ) to 8.36 \pm 1.08 % (MED-EL FlexSoft) when the Cole-Cole approximation was used and between 3.24 \pm 0.90 % (AB HiFocus SlimJ) to 7.36 \pm 1.14 % (MED-EL FlexSoft) for the Schwan-Faraday model. Thus, both approaches showed no significant

MED-EL FlexSoft (SE3 vs SE4)

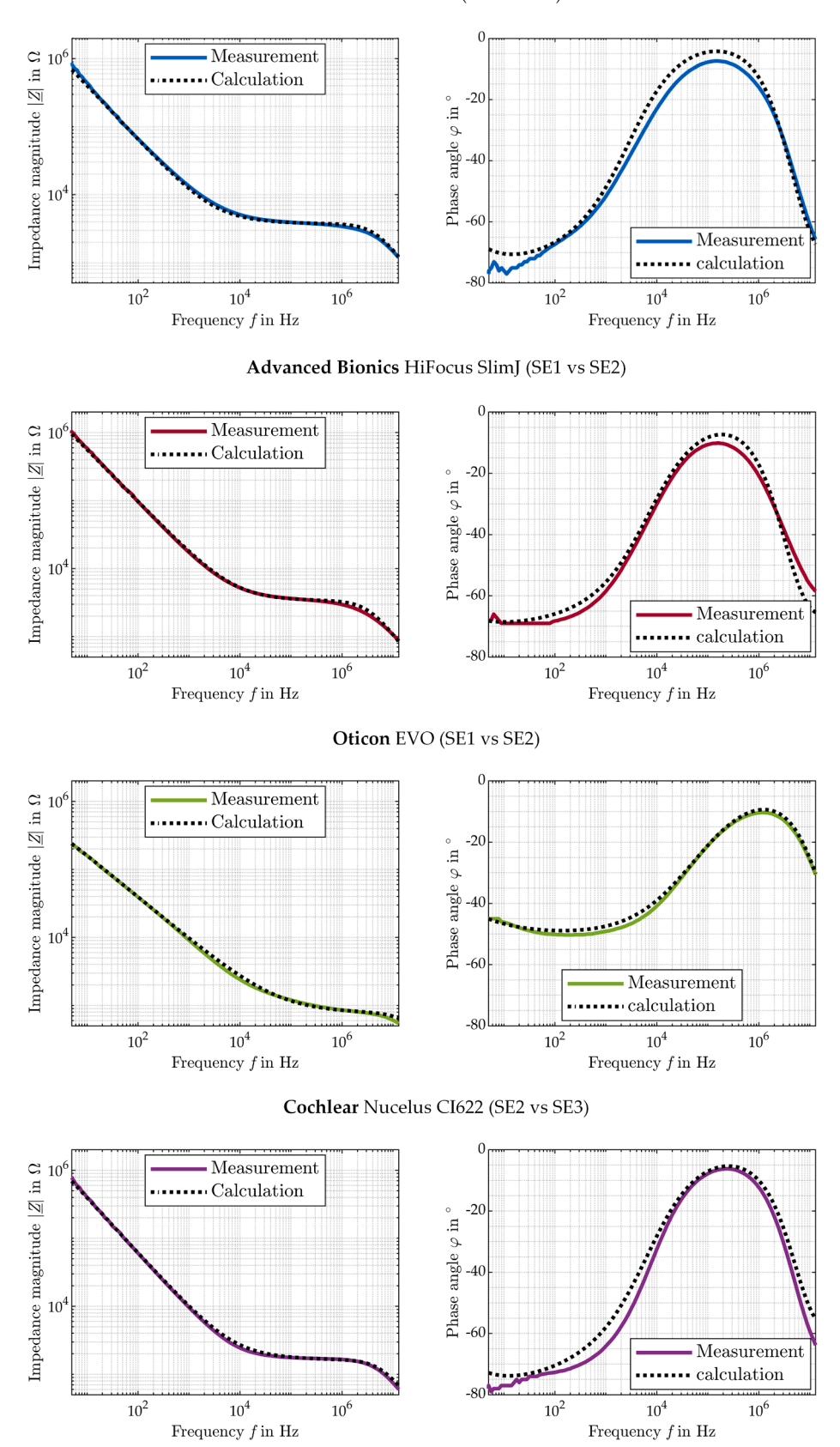


Fig. 10. Correspondence between the calculated (black dotted lines) impedance magnitude |Z| and phase angle φ and the measurement data (colored solid lines) using the Schwan-Faraday bilayer model. As an example, the most apical intact SE combination of the four CI electrodes MED-EL FlexSoft (blue), AB HiFocus SlimJ (red), Oticon EVO (green) and Cochlear Nucleus CI622 (purple) is shown.

Table 6

Average errors across all neighboring SE combinations for the calculation of complex impedance, magnitude and phase angle related to the measured values over the whole frequency spectrum with a Schwan-Faraday bilayer model.

Errors (average across all frequencies)		MED-EL FlexSoft	Advanced Bionics HiFocus SlimJ	Oticon EVO	Cochlear Nucleus CI622
Most apical SE combination	Magnitude \overline{e}_Z [%]	5.05 ± 3.57	3.64 ± 3.88	5.05 ± 5.25	4.33 ± 3.73
	Phase angle \overline{e}_{φ} [$^{\circ}$]	3.24 ± 1.67	2.63 ± 1.64	1.04 ± 0.61	3.56 ± 2.20
	Complex impedance $\overline{e}_{\underline{z}}$ [%]	8.04 ± 3.47	6.53 ± 3.98	$\textbf{5.67} \pm \textbf{5.07}$	8.01 ± 5.00
Average of all neighboring SE combinations	Magnitude $\overline{\overline{e}_Z}$ [%]	7.36 ± 1.14	3.24 ± 0.90	5.12 ± 1.47	4.00 ± 1.10
	Phase angle $\overline{\overline{e}_{\omega}}$ [°]	3.46 ± 0.47	2.57 ± 0.85	3.84 ± 1.83	3.20 ± 0.86
	Complex impedance $\overline{\overline{e_Z}}$ [%]	10.41 ± 1.26	6.03 ± 1.78	$\textbf{9.32} \pm \textbf{3.19}$	7.36 ± 1.77

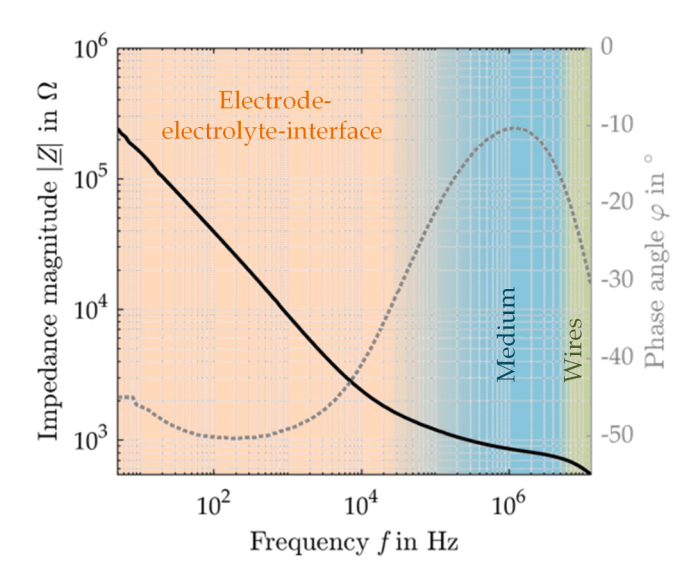
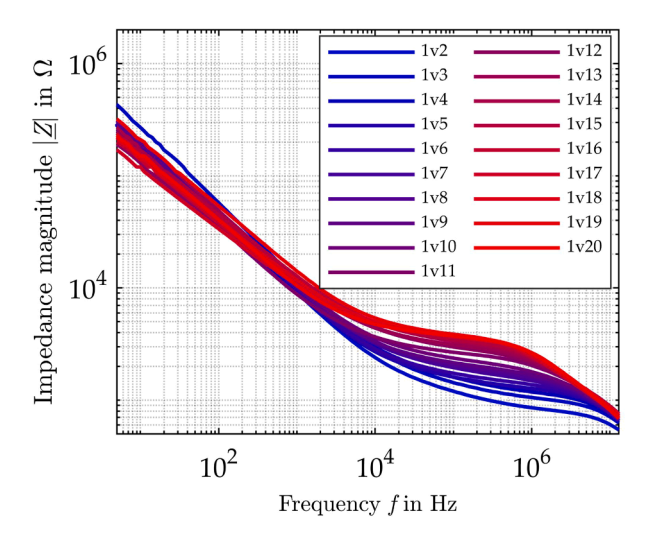


Fig. 11. Exemplary measurement of the impedance between SE1 and SE2 of the Oticon EVO electrode. Magnitude of impedance $|\underline{Z}|$ (black, solid) and phase angle φ (grey, dotted). The measurement shows a non-linear low frequency range (orange), where the electrode-electrolyte interface dominates, a close-to-resistive (with a maximum phase angle around 1 MHz, blue) and mid-frequency range before the (wire) capacitances start to become effective at high frequencies (green).

difference in performance to model the impedance magnitude. Relative average errors in phase (eq. (2)) across all frequencies remained below 5.59° for all models and electrode types.

To investigate the ability of both models to capture the measurement data, additionally, a statistic analysis for different frequency ranges was performed (supplementary information Table S4 and S5). Mean errors in impedance (eq. (3).) were usually less at low frequencies, where also an advantage of the Schwan-Faraday model was apparent to capture low frequency features. Moreover, errors were usually significant for frequencies > 1 MHz indicating that the simplified network assumed in this study might be less appropriate at high frequencies.

A typical biphasic pulse with 25 µs phase duration and 7 µs interphase gap has a fundamental frequency of approximately 16 kHz and higher harmonics. Thus, currently available CIs mainly convey energy in the mid and high frequency range between 10 kHz and 13 MHz and would be mostly affected by the electrolyte and electrical properties of the CI electrode, such as wire arrangement and SE geometry. To enable the full potential of precision impedance spectroscopy to differentiate cell types [15], sufficient coverage of the measuring signal over an extended frequency range is required. Varying the pulse repetition rate in existing CIs could be a possibility to implement a close to conventional impedance spectroscopy. E.g. in Cochlear Ltd. devices, it is possible to vary the frequency in the fitting software between 250 and 1800 pulses per second by increasing the time between two pulses. In principle this allows the extension to lower frequencies of the stimulation frequency, but usually not as a continuous band. Similar medical devices with adequate size for implants show that continuous stimulation frequencies up to 0.2 MHz can be used for impedance spectroscopy in the body [43]. Hence, appropriate circuits might be integrated into current devices covering the frequency range up to a few hundred kHz



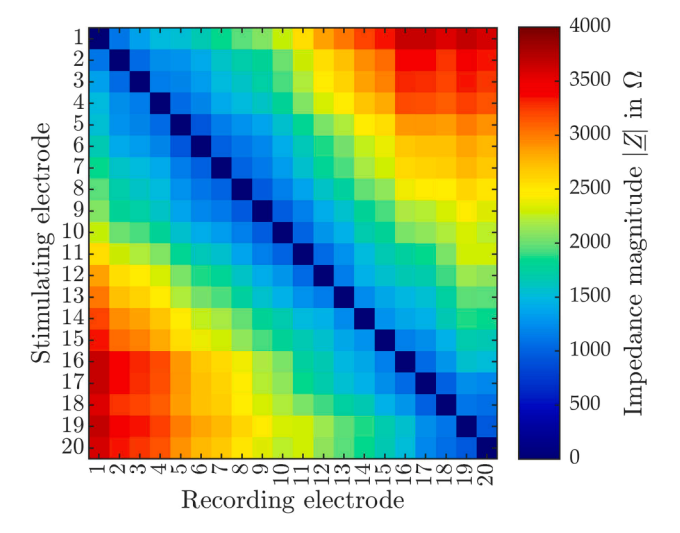


Fig. 12. Left: Impedance magnitude $|\underline{Z}|$ measurement of the Oticon EVO electrode between 5 Hz and 13 MHz for all stimulation electrodes versus the most apical stimulation electrode SE1. Measurements were performed in a straight cylindrical volume of 1.2 mm diameter filled with artificial perilymph of 14.92 mS/cm conductivity. Right: Impedance matrix derived from an estimate of the resistive part (avg. $|\underline{Z}|$ between 50 kHz - 500 kHz).

with reasonable accuracy. Although possible, the latter is not implemented in current CIs. Thus, the possible range of pulse duration variation and its resulting frequency restrict the implementation in today's devices.

Here we addressed the impact on impedances measured with several electrode arrays using a simple electrical equivalent circuit with two non-linear bilayer models in a 2-pole configuration. Although, measurements against a reference are common, a 2-pole setup has the advantage that it can be used in a defined environment with the best spatial resolution to study the basic properties. Common reference electrodes include the unknown properties of the return pathway [16-18] and a geometrical model of the cochlea surrounding, whereas 4-pole configurations suffer from the necessity to model the current pathway [20]. Our approach allows to determine the variables that constitute this underdetermined system, such as wire resistance and crosstalk. Both can be measured before implantation as these are unlikely to change over time. The other properties can be determined by the 2-pole impedance spectroscopy with a reasonable accuracy of approximately 10 % in all investigated electrodes. Further the Schwan-Faraday bilayer model describes the measurement data slightly better than the Cole-Cole bilayer model. Moreover, in contrast to stimulation against a common reference electrode, it allows the estimation of the capacitive interaction between connections, independent of the pathway along the cochlea.

However, some compromises in our approach were made and possibly the accuracy can be increased further. Firstly, the 2-pole EEC may be too simple to describe some properties in detail. For example, the wire capacity and resistance will be distributed and a transmission line model may be more appropriate. Secondly, for calculation of the effective wire resistance and capacitance, different sections, such as the wiring in the connector, in the leads to the electrode array and in the electrode array were not distinguished. Here a distinction between different sections may be helpful to separate their respective contributions. Thirdly, in the scope of the present study only neighboring SE combinations were considered. As can be seen in measurements that bridge more than neighbors (see Fig. 12) not only the resistance of the medium is increased, but equally the high frequency roll-off and its corner frequency. This and the increased error at high frequencies is an indicator that beside the capacitive pathway the entire resistive pathway contributes and has to be considered as a whole. Nevertheless, the introduced simplified EEC is with an accuracy of approximately 10 % a good basis for further optimization.

The presence of different tissues and cells around the electrode affects the impedance spectrum, allowing for the differentiation between fibrotic and normal tissue [44]. One bottleneck for CIs is the impact of the electrical properties of the electrode array itself on the measurements that was addressed here. As a first step, our model is able to determine this influence of CI electrode arrays on impedance spectroscopy measurement results. However, differentiating between cell types using our model can be quite complex due to the overlapping electrical properties of tissues that also need to be characterized, i.e. the presence of fibrosis introduces additional components to our model. General model adjustments like parameter estimation, adding new components and further model optimization would be required and intended by us in the future.

Nevertheless, the determination of system parameters, such as the wire resistance and cross-capacitance needs to be conducted before implantation in our approach. As this is currently not performed during manufacturing and specifications are not publically available the alternative is the estimation of system parameters. In this aspect our study is limited as we had only one CI electrode of each design for testing. As shown in Fig. 6, right and Figure S1, wire resistances per length for the different stimulation electrodes are nearly constant in each type of all investigated CIs. Same applies for the cross capacitances per length (Fig. 7, right and Figure S2). These findings can be used as an estimate for implanted devices as well, using the resistances and cross

capacitances per length as an estimate for the EEC's parameters $R_{\rm wa}$, $R_{\rm wb}$ and $C_{\rm ab}$. For other types of CIs, these parameters have to be determined and provided, e.g. by the manufacturer. However, to generalize it for other designs and to make a substantiated statement on the expected distribution and variability of system parameters, a larger sample size of same electrode types needs to be tested. Moreover, the impact of the reduced accuracy on measurement results needs to be investigated if system parameters are replaced by statistical estimates in already implanted or future devices.

Although we could characterize and model the electrical properties with sufficient accuracy and the technical integration of impedance spectroscopy into cochlear implants appears feasible, the legal requirements for an active class III device are not straightforward and the effort of implementation requires a prior good justification.

5. Conclusion

In conclusion, our study developed and validated an electrical equivalent circuit (EEC) model to describe the basic electric properties of cochlear implant (CI) electrode arrays in a 2-pole configuration using precision impedance spectroscopy. We addressed the underdetermined nature of the system by measuring lacking parameters independently in four commercial CI electrode arrays and by incorporating linear elements and comparing two common electrochemical bilayer models (Cole-Cole and Schwan-Faraday). The model accurately captured the impedance characteristics across a frequencies range between 5 Hz - 13 MHz, revealing distinct frequency domains influenced by the bilayer and resistive and capacitive properties of the arrays. Although the simplified EEC provided approximately 10 % accuracy, further refinement, optimization, and more comprehensive consideration of electrode array sections, could enhance precision. Our findings also underscore the potential of integrating impedance spectroscopy into CIs for advanced diagnostics, though technical, manufacturing, and regulatory challenges remain.

Funding

This work has been funded by the Deutsche Forschungsgemeinschaft (German Research Foundation) SFB/TRR 298 SIIRI Project ID 426335750 as well as under Germany's Excellence Strategy EXC 2177/1 Project ID 390895286.

CRediT authorship contribution statement

Merle Sehlmeyer: Writing – review & editing, Writing – original draft, Visualization, Validation, Methodology, Investigation, Formal analysis, Data curation. Mit B. Bhavsar: Writing – original draft, Methodology, Investigation, Formal analysis, Data curation, Writing – review & editing, Validation, Visualization. Stefan Zimmermann: Writing – review & editing, Validation, Supervision, Project administration, Funding acquisition, Conceptualization. Hannes Maier: Writing – review & editing, Writing – original draft, Validation, Supervision, Project administration, Methodology, Funding acquisition, Conceptualization.

Declaration of competing interests

The authors declare that they have no known competing financial interests or personal relationships that could have appeared to influence the work reported in this paper.

Data availability

Data will be made available on request.

Acknowledgments

We thank MED-EL Medical Electronics GmbH (MED-EL, Innsbruck, Austria), Advanced Bionics LLC (AB, Valencia, CA, USA), Oticon Medical/Neurelec SAS (Oticon, Vallauris, France) and Cochlear Ltd. (Cochlear, Sydney, Australia) for the donation of cochlear implant electrodes

Also, we thank Maren Prediger (IMPT, LUH) and Antoly Glukhovskoy (IMPT, LUH) for the connection of the cochlear implants to an adapter, Kai Tönnies (central research workshops, MHH) for PCB design and Alexander Nitschke (GEM, LUH) and Peter Erfurt (NIFE) for support with microscopy.

Supplementary materials

Supplementary material associated with this article can be found, in the online version, at doi:10.1016/j.heares.2024.109125.

References

- [1] W.H.O., World report on hearing, 2021. https://www.who.int/publications/i/item/world-report-on-hearing (accessed 6 March 2021).
- [2] W.H.O., Deafness and hearing loss., 2024. https://www.who.int/news-room/fact-sheets/detail/deafness-and-hearing-loss (accessed 15 May 2024).
- [3] Boisvert, I., Reis, M., Au, A., Cowan, R., Dowell, R.C., 2020. Cochlear implantation outcomes in adults: a scoping review. PLoS ONE 15, e0232421. https://doi.org/ 10.1371/journal.pone.0232421
- [4] Firszt, J.B., Koch, D.B., Downing, M., Litvak, L., 2007. Current steering creates additional pitch percepts in adult cochlear implant recipients. Otol. Neurotol. 28, 629–636. https://doi.org/10.1097/01.mao.0000281803.36574.bc.
- [5] Campbell, A.P., Suberman, T.A., Buchman, C.A., Fitzpatrick, D.C., Adunka, O.F., 2010. Correlation of early auditory potentials and intracochlear electrode insertion properties: an animal model featuring near real-time monitoring. Otol. Neurotol. 31, 1391–1398. https://doi.org/10.1097/MAO.0b013e3181f6c899.
- [6] Shallop, J.K., Facer, G.W., Peterson, A., 1999. Neural response telemetry with the nucleus CI24M cochlear implant. Laryngoscope 109, 1755–1759. https://doi.org/ 10.1097/00005537-199911000-00006.
- [7] Bester, C., Razmovski, T., Collins, A., Mejia, O., Foghsgaard, S., Mitchell-Innes, A., Shaul, C., Campbell, L., Eastwood, H., O'Leary, S., 2020. Four-point impedance as a biomarker for bleeding during cochlear implantation. Sci. Rep. 10, 2777. https://doi.org/10.1038/s41598-019-56253-w.
- [8] Aebischer, P., Meyer, S., Caversaccio, M., Wimmer, W., 2021. Intraoperative impedance-based estimation of cochlear implant electrode array insertion depth. IEEE Trans. Biomed. Eng. 68, 545–555. https://doi.org/10.1109/ TBME.2020.3006934.
- [9] Newbold, C., Richardson, R., Millard, R., Huang, C., Milojevic, D., Shepherd, R., Cowan, R., 2010. Changes in biphasic electrode impedance with protein adsorption and cell growth. J. Neural Eng. 7, 56011. https://doi.org/10.1088/1741-2560/7/ 5/056011.
- [10] Wilk, M., Hessler, R., Mugridge, K., Jolly, C., Fehr, M., Lenarz, T., Scheper, V., 2016. Impedance changes and fibrous tissue growth after cochlear implantation are correlated and can be reduced using a dexamethasone eluting electrode. PLoS ONE 11, e0147552. https://doi.org/10.1371/journal.pone.0147552.
- [11] Hans, S., Arweiler-Harbeck, D., Kaster, F., Ludwig, J., Hagedorn, E., Lang, S., Meyer, M., Holtmann, L.C., 2021. Transimpedance matrix measurements reliably detect electrode tip fold-over in cochlear implantation. Otol. Neurotol. 42, e1494–e1502. https://doi.org/10.1097/mao.000000000003334.
- [12] Leblans, M., Zarowski, A., Molisz, A., van Dinther, J., Dedeyne, J., Lerut, B., Kuhweide, R., Offeciers, E., 2023. Cochlear implant electrode array tip-foldover detection by electrode voltage telemetry. Cochlear Implants Int 24, 95–106. https://doi.org/10.1080/14670100.2022.2148890.
- [13] de Rijk, S.R., Hammond-Kenny, A., Tam, Y.C., Eitutis, S.T., Garcia, C., Carlyon, R. P., Bance, M., 2022. Detection of extracochlear electrodes using stimulation-current- induced non-stimulating electrode voltage recordings with different electrode designs. Otol. Neurotol. 43, e548–e557. https://doi.org/10.1097/MAQ.0000000000003512.
- [14] Zhang, L., Schmidt, F.H., Oberhoffner, T., Ehrt, K., Cantré, D., Großmann, W., Schraven, S.P., Mlynski, R., 2024. Transimpedance matrix can be used to estimate electrode positions intraoperatively and to monitor their positional changes postoperatively in cochlear implant patients. Otol. Neurotol. 45, e289–e296. https://doi.org/10.1097/mao.0000000000004145.
- [15] Foster, K.R., Schwan, H., 2019. Dielectric permitivity and electric conductivity of biological materials. In: Polk, C., Postow, E. (Eds.), CRC Handbook of Biological Effects of Electromagnetic fields, Secondnd. CRC Press, Boca Raton, pp. 25–102, 1986.
- [16] Frijns, J.H., de Snoo, S.L., Schoonhoven, R., 1995. Potential distributions and neural excitation patterns in a rotationally symmetric model of the electrically

- stimulated cochlea. Hear. Res. 87, 170–186. https://doi.org/10.1016/0378-5955 (95)00090-O.
- [17] Kalkman, R.K., Briaire, J.J., Frijns, J.H.M., 2016. Stimulation strategies and electrode design in computational models of the electrically stimulated cochlea: an overview of existing literature. Network 27, 107–134. https://doi.org/10.3109/ 0954898X.2016.1171412.
- [18] Nogueira, W., Schurzig, D., Büchner, A., Penninger, R.T., Würfel, W., 2016. Validation of a cochlear implant patient-specific model of the voltage distribution in a clinical setting. Front. Bioeng. Biotechnol. 4, 84. https://doi.org/10.3389/ fbioe.2016.00084.
- [19] Molaee-Ardekani, B., Donahue, M.J., 2023. Investigating the electrode-electrolyte interface modelling in cochlear implants. Biomed. Phys. Eng. Express. https://doi. org/10.1088/2057-1976/aceafb.
- [20] Razmovski, T., Collins, A., Bester, C., O'Leary, S., 2023. Using four-point impedance to detect and locate blood during cochlear implantation. Annu. Int. Conf. IEEE Eng. Med. Biol. Soc. 2023, 1–4. https://doi.org/10.1109/ EMBC40787.2023.10340312.
- [21] MED-EL Medical Electronics, FLEX electrode arrays: right fit for each cochlea, 2021.
- [22] Dhanasingh, A., 2021. The rationale for FLEX (cochlear implant) electrode with varying array lengths. World J. Otorhinolaryngol. Head Neck Surg. 7, 45–53. https://doi.org/10.1016/j.wjorl.2019.12.003.
- [23] Advanced bionics LLC and affiliates., Surgeon's Manual for the HiRes™ Ultra 3D: cochlear Implant with the HiFocus™ SlimJ and HiFocus™ Mid-Scala Electrodes, 2021.
- [24] Oticon Medical, Neuro Zti cochlear implant range: cochlear implant system product information.
- [25] Oticon Medical, Soft surgery with EVO® electrode array preserves residual hearing, 2024. https://www.oticonmedical.com/de/for-professionals/cochlear-i mplant/clinical-results/soft-surgery-with-evo-electrode-array-preserves-resi dual-hearing (accessed 14 March 2024).
- [26] Cochlear Limited, 2022. Cochlear™ Nucleus® CI622 Cochlear Implant with Slim Straight Electrode.
- [27] Cochlear Limited, 2019. Cochlear ™ Nucleus® Profile™ Plus with Slim Straight Electrode (CI622): Technical Specifications.
- [28] Prasad, S., Vona, B., Diñeiro, M., Costales, M., González-Aguado, R., Fontalba, A., Diego-Pérez, C., Subasioglu, A., Bademci, G., Tekin, M., Cabanillas, R., Cadiñanos, J., Fridberger, A., 2020. Radixin modulates the function of outer hair cell stereocilia. Commun. Biol. 3, 792. https://doi.org/10.1038/s42003-020-01506-y.
- [29] Agilent Technologies, 4192A LF impedance analyzer operating and service manual, 2000.
- [30] Michael D Kelzenberg, Impedance Analysis Software, Pasadena, CA.
- [31] Sehlmeyer, M., Bhavsar, M.B., Biebighaeuser, J., Hitzemann, M., Maier, H., Lippmann, M., Schaefer, C., Zimmermann, S., 2023. Impedance spectroscopy of enlarged cochlear implant stimulation electrodes – FEM simulations considering the perilymph. tm - Technisches Messen 90, 809–821. https://doi.org/10.1515/ teme-2023-0091
- [32] Cole, K.S., Cole, R.H., 1941. Dispersion and absorption in dielectrics I. alternating current characteristics. J Chem Phys 9, 341–351. https://doi.org/10.1063/ 1.1750906
- [33] Lasia, A., 2014. Electrochemical Impedance Spectroscopy and Its Applications. Springer New York, New York, NY.
- [34] Zoltowski, P., 1998. On the electrical capacitance of interfaces exhibiting constant phase element behaviour. J. Electroanalyt. Chem. 443, 149–154. https://doi.org/ 10.1016/S0022-0728(97)00490-7.
- [35] Schwan, H.P., 1957. Electrical properties of tissue and cell suspensions. Adv. Biol. Med. Phys. 5, 147–209. https://doi.org/10.1016/B978-1-4832-3111-2.50008-0.
- [36] Kral, A., Aplin, F., Maier, H., 2021. Prostheses for the Brain: Introduction to Neuroprosthetics. Elsevier Science & Technology, San Diego.
- [37] Schwan, H.P., 1992. Linear and nonlinear electrode polarization and biological materials. Ann. Biomed. Eng. 20, 269–288. https://doi.org/10.1007/BF02368531.
- [38] Fricke, H., 1932. XXXIII. The theory of electrolytic polarization. London, Edinburgh, Dublin Philos. Mag. J. Sci. 14, 310–318. https://doi.org/10.1080/ 14786443209462064
- [39] Brummer, S.B., Turner, M.J., 1975. Electrochemical behavior of platinum-saline interface. J. Electrochem. Soc. C109. -C109.
- [40] Lasia, A., 2022. The origin of the constant phase element. J. Phys. Chem. Lett. 13, 580–589. https://doi.org/10.1021/acs.jpclett.1c03782.
- [41] Tsai, P.J., Nayak, S., Ghosh, S., Puri, I.K., 2017. Influence of particle arrangement on the permittivity of an elastomeric composite. AIP Adv. 7, 015003. https://doi. org/10.1063/1.4973724.
- [42] Kaatze, U., 1997. The dielectric properties of water in its different states of interaction. J. Sol. Chem. 26, 1049–1112. https://doi.org/10.1007/BF02768829.
- (43] N. Goll, The world's smallest impedance spectroscopy system in the form of a pill finds weak spots in machines and people. https://www.izm.fraunhofer.de/en/new s_events/tech_news/the-world-s-smallest-impedance-spectroscopy-system.html (accessed 27 July 2024).
- [44] de Rijk, S.R., Boys, A.J., Roberts, I.V., Jiang, C., Garcia, C., Owens, R.M., Bance, M., 2023. Tissue-engineered cochlear fibrosis model links complex impedance to fibrosis formation for cochlear implant patients. Adv. Healthc. Mater. 12, e2300732. https://doi.org/10.1002/adhm.202300732.